

We are IntechOpen, the world's leading publisher of Open Access books Built by scientists, for scientists

5,800

Open access books available

142,000

International authors and editors

180M

Downloads

Our authors are among the

154

Countries delivered to

TOP 1%

most cited scientists

12.2%

Contributors from top 500 universities



WEB OF SCIENCE™

Selection of our books indexed in the Book Citation Index
in Web of Science™ Core Collection (BKCI)

Interested in publishing with us?
Contact book.department@intechopen.com

Numbers displayed above are based on latest data collected.
For more information visit www.intechopen.com



CFD Combustion Simulations and Experiments on the Blended Biodiesel Two-Phase Engine Flows

*Vinay Atgur, Gowda Manavendra,
Gururaj Pandurangarao Desai
and Boggarapu Nageswara Rao*

Abstract

Biodiesels are the promising sources of alternative energy. Combustion phenomenon of blended biodiesels differs to those of diesel due to changes in physio-chemical properties. Experimental investigations are costly and time-consuming process, whereas mathematical modeling of the reactive flows is involved. This chapter deals with combustion simulations on four-stroke single-cylinder direct injection compression ignition engine running at a constant speed of 1500 rpm, injection timing of 25° BTDC with diesel and 20% blend of Jatropha biodiesel. Standard finite volume method of computational fluid dynamics (CFD) is capable of simulating two-phase engine flows by solving three-dimensional Navier–Stokes equations with $k-\epsilon$ turbulence model. Combustion simulations have been carried out for half-cycle by considering the two strokes compression and expansion at zero load condition. The model mesh consists of 557,558 elements with 526,808 nodes. Fuel injection begins at 725° and continues till 748° of the crank angle. Charge motion within the cylinder, turbulent kinetic energy, peak pressure, penetration length, and apparent heat release rate are analyzed with respect to the crank angle for diesel and its B-20 Jatropha blend. Experimental data supports the simulation results. B-20 Jatropha blend possesses similar characteristics of diesel and serves as an alternative to diesel.

Keywords: combustion, simulation, crank angle, compression, fuel spray

1. Introduction

Combustion plays a vital role in the chemical, electrical and transportation industries [1–3].

Understanding of the combustion phenomenon through experimentation is involved and expensive. In such situations, numerical simulations act as an alternative platform. There is a need to develop mathematical models for the reactive flows. Due to variation of density, the heat transfer and fluid motion inside the engine is unsteady and turbulent. Most of the simplified real process versions are based on the idealization of the cylindrical geometry models. Combustion

phenomenon is greatly influenced by fuel properties, fuel preparation and fuel distribution inside the cylinder. The advancement in computer technology is helpful in solving the complicated equations relevant to the turbulence-chemistry interactions.

Jafarmadar and Zehni [4] have studied the high-speed diesel engine combustion using AVL-FIRE code CFD. They have analyzed the peak pressure rise and heat release rate. They have made comparison of numerical simulations with experiments varying the fuel injection pressure. The KIVA group of codes will be helpful in performing diesel engine simulations with less computational time. The enhanced code and coarse meshes are utilized to simulate combustion in a heavy-duty Mitsubishi Heavy Industries diesel engine for the service loads, speeds, and injection pressure. The normal simulation time from IVC to EVO is reduced from 60 hours to 1 hour using 12 processors [5]. Various researchers have developed alternative codes and models for minimizing the simulation time of combustion [6–8].

Mirko Baratta et al. [9] have utilized CFD models and analyzed laminar flame speed for different fuel composition and mixture dilution rates. Michela Costa et al. [10] have performed simulations on premixed syngas and biodiesel as pilot injection. The combustion efficiency decreases, exhaust gas temperature and thermal efficiency increase with increasing the % of syngas. The reduced chemical kinetics model gives an improved solution. Amin Maghbouli et al. [11] have used a 3D-CFD/Chemical kinetics framework model to investigate the diesel engine/gas dual-fuel engine combustion process. Methane and n-heptane are used as natural gas representatives. Source terms in conservation equations of energy and species are calculated by integrating CHEMKIN solver into KIVA code. Pressure, ignition delay and heat release rate are in good agreement with experiments. Vijayshree and Ganesan [12] have performed CFD simulations for designing IC engine through combustion process analysis.

CFD studies thus provide flow visualization, optimal engine parameters and knowledge in combustion phenomenon, which are difficult to acquire from experiments. Experimental investigations are involved in obtaining the penetration length, velocity distribution, swirl ratio, tumble ratio and heat release rate. Modifications in engine design and parameters are difficult to implement. The task will be definitely a time-consuming process. CFD serves as a versatile and powerful tool for designing IC engine and gives insight into the complex fluid dynamics. Experiments on various blends (5–30%) indicate B-20 blend as viable in terms of performance and emission. Combustion simulations help in minimizing engine bench tests.

Comparative studies are made in this article to examine the combustion behaviour of diesel and B-20 blend of Jatropa. Combustion simulations have been performed utilizing ANSYS Fluent 15.0 version. Combustion simulations are in line with those of DSC (differential scanning calorimetry) analysis with a heating rate of 10°C/min in atmospheric air.

2. Modeling and simulations

This section deals with the combustion simulations on the four-stroke single-cylinder direct injection compression ignition engine running at a constant speed of 1500 rpm, injection timing of 25° BTDC with diesel and 20% blend of Jatropa biodiesel. Standard finite volume method of computational fluid dynamics (CFD) is capable of simulating the two-phase engine flow. Three-dimensional Navier–Stokes equations are solved with k - ϵ turbulence model. The details of combustion simulations carried out for half-cycle by considering the two strokes compression and

expansion at zero load condition are presented below. **Figure 1** shows the front view and 3D view of the geometry model. The model is a four-stroke diesel engine with 4 valves and 4 ports for air sucking inlets and hot gas outlets. The green portion in **Figure 1** is the assembly of a cylinder and piston. Specifications are made from the standard engine KIRLOSKAR AV-1 model. The mathematical models in CFD begin with representation of combustion chamber geometry (meshing of engine). The meshing of the geometry model **Figure 2** is generated using the pre-processor of ANSYS Fluent 15.0 version.

The fluid chamber bottom of ICE is modelled with 450,570 elements and 470,654 nodes. The fluid chamber top of ICE is modelled with 9795 elements and 13,544 nodes. Fluid piston of ICE is modelled with 66,443 elements and 73,360 nodes. The model domain consists of 526,808 elements and 557,558 nodes. Mesh

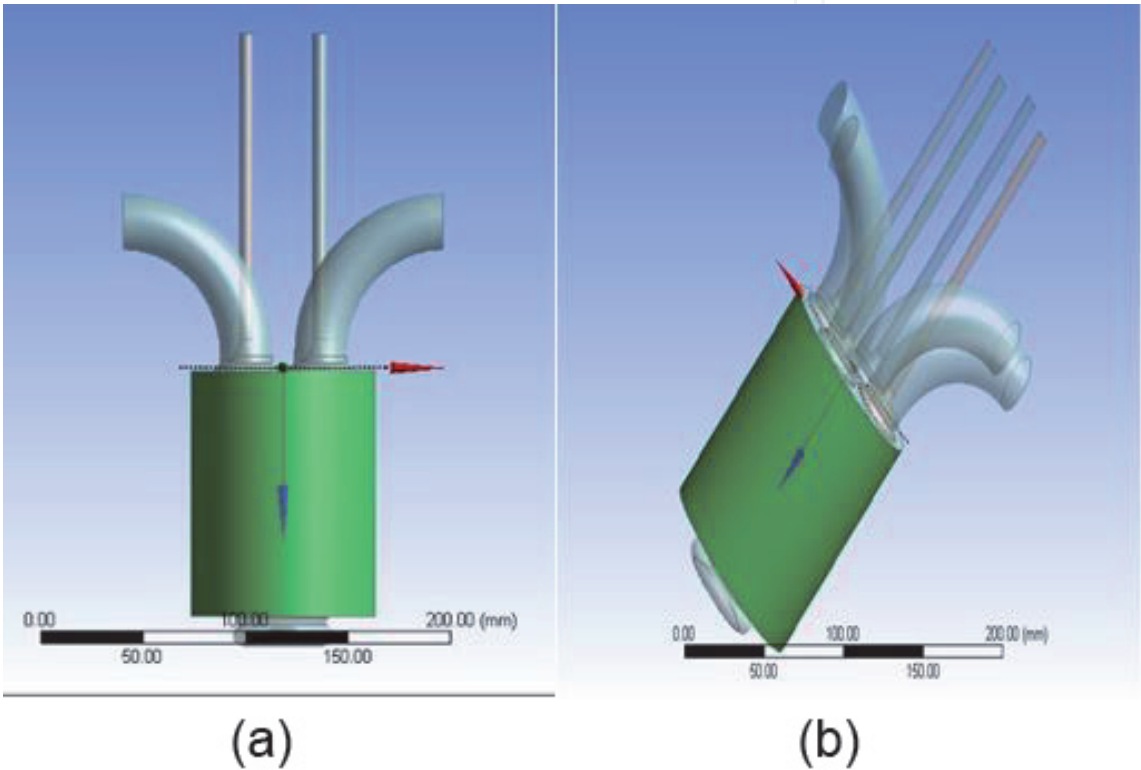


Figure 1.
Geometry model. (a) Front view. (b) 3D view.

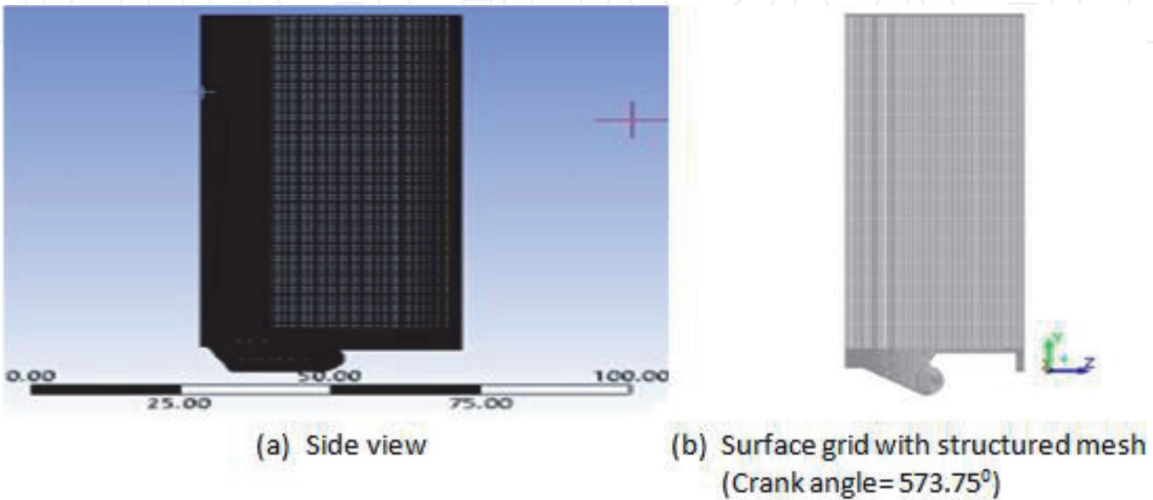


Figure 2.
Geometry mesh.

parameters of IC sector are: Reference size = 0.947 mm; Minimum mesh size = 0.19 mm; Maximum mesh size = 0.474 mm; and the chamber body mesh size = 1.487 mm with 3 inflation layers.

The complex physical phenomenon of combustion flows in IC engines (see **Figure 2**) can be understood by solving the following 3-Dimensional Navier-Stokes (N-S) equations with the Reynold's Average Navier-Stokes (RANS) model [13–15] and the k-ε turbulence model [16, 17].

N-S equations:

$$\frac{\partial v_j}{\partial x_j} = 0 \quad (1)$$

$$\rho \left(\frac{\partial v_i}{\partial t} + v_j \frac{\partial v_i}{\partial x_j} \right) = -\frac{\partial P}{\partial x_i} + \mu \frac{\partial}{\partial x_j} \left(\frac{\partial v_i}{\partial x_j} \right) \quad (2)$$

RANS model:

$$\frac{\partial \bar{v}_i}{\partial x_j} = 0 \quad (3)$$

$$\rho \left(\frac{\partial \bar{v}_i}{\partial t} + \bar{v}_j \frac{\partial \bar{v}_i}{\partial x_j} \right) = \frac{\partial \bar{P}}{\partial x_i} + \mu \frac{\partial}{\partial x_j} \left(\frac{\partial \bar{v}_i}{\partial x_j} \right) - \rho \frac{\partial \bar{u}_i' u_j'}{\partial x_j} \quad (4)$$

$$-\rho \bar{u}_i' u_j' = \mu_t \left(\frac{\partial \bar{v}_i}{\partial x_j} + \frac{\partial \bar{v}_j}{\partial x_i} \right) \quad (5)$$

$$\rho \left(\frac{\partial \bar{v}_i}{\partial t} + \frac{\partial \bar{v}_i}{\partial x_j} \right) = -\frac{\partial \bar{P}}{\partial x_i} + \frac{\partial}{\partial x_j} \left[(\mu + \mu_t) \left(\frac{\partial \bar{v}_i}{\partial x_j} \right) \right] \quad (6)$$

k-ε turbulence model:

$$\rho \left(\frac{\partial k}{\partial t} + \frac{\partial (k v_j)}{\partial x_j} \right) = \frac{\partial}{\partial x_j} \left[\left(\mu + \frac{\mu_t}{\sigma_k} \right) \frac{\partial k}{\partial x_j} \right] + \mu_t \gamma^2 - \rho \xi \quad (7)$$

Here ρ is density; μ is dynamic viscosity; u and v are velocity components in x and y directions; p refers to pressure; μ_t is the eddy or turbulent viscosity; ξ is the rate of heat dissipation; k is the turbulent kinetic energy; $\sigma_k \approx 1$, is model constant. The RANS models are created with variations referred to over bars and apostrophes in Eqs. (3)–(6) for incompressible fluids. Eqs. (5) and (6) are used for evaluating the Reynolds 'stress equivalent to the average gradients of velocity (equivalent to shear stress). The k-ε turbulence model (7) will be used for the gas and liquid phase [18].

Finite volume equations are crucial for CFD simulations to handle fluid boundary layers on surfaces [19, 20]. The shear gap is heavily influenced by boundary conditions. Fluid near the wall (i.e., layer close to the wall) is the viscous sub-layer, whereas above this layer is dominated by turbulent shears. The laminar pressure-stress relation is

$$\frac{v C_\mu^{0.25} k^{0.25}}{\frac{\tau_w}{\rho}} = v^* = y^* = \frac{\rho C_\mu^{0.25} k^{0.25} y}{\mu} \quad (8)$$

Here y is the cell's close-to-wall position; v is the medium fluid speed; and C_μ is nearly equal to 0.09. It is more precise to calculate near-wall gradients using constrained equivalences when the laminar stress-strain relationship is important.

The near-wall grid involves substantially larger number of cells, which increases computational time.

The temperature at the ICE-cylindrical chamber bottom and top surfaces is 567 K. The ICE-cylindrical-piston wall temperature is also specified as 567 K. The wall temperature of ICE-piston is 645 K. The wall temperature is 602 K on ICE-sector-top-faces. Relaxation of crank angles are: Engine speed = 1500 rev/min.; Crank radius = 55 mm; Piston pin-offset = 0 mm; Connecting rod length = 165 mm; Cylinder bore length = 110 mm; and Cylinder bore diameter = 90 mm. **Table 1**

Parameter	Dimension
X-Position	0
Y-Position	−0.00012
Z-Position	2E-05
X-Axis	0
Y-Axis	−0.34202
Z-Axis	0.939693
Diameter (m)	2.54E-4
Evaporating Species	C ₇ h ₁₆
Temperature (K)	366.7
Start Crank Angle (deg)	721
End Crank Angle (deg)	742.5
Cone Angles (deg)	9
Cone Radius (deg)	1.27E-4
Total Flow Rate (kg/s)	1.3333E-05
Velocity Magnitude (m/s)	468

Table 1.
Injection Properties.

Fuel	Calorific value (MJ/kg)	Kinematic Viscosity @40°C (cst)	Cetane value	Density (kg/m ³)	Flash point (°C)	Pour point (°C)	Cloud point (°C)
DIESEL	44.22	2.87	47.8	840	76	−3	6.5
JOME	39.79	4.73	52	862.2	182.5	3	3
B-20JOME	44.10	3.99	49	840.2	93.5	−3	4

Table 2.
Biodiesel and diesel properties [2].

Fuel	Thermal Conductivity (W/mk)	Specific Heat (MJ/m ³ K)	Thermal Diffusivity (mm ² /s)
Diesel	0.3390	0.2563	1.323
JOME	0.2537	0.5773	0.4083
B-20 JOME	0.3090	0.3894	0.7934

Table 3.
Thermo-physical properties of diesel and biodiesel.

provides the injection properties. **Tables 2** and **3** provide thermo-physical properties of diesel, Jatropha oil methyl ester (JOME) and its B-20 blend for combustion simulations. The properties are measured from TPS 500S with Kapton and Teflon sensors.

Fuel starts to penetrate into the combustion chamber at 728°C for the diesel as well as biodiesel. Due to the high viscosity of the B-20 Jatropha leads to poor atomization. As in [21], the temperature rise during the fuel spray is around 2770°C for diesel and 2670°C for biodiesel (see **Figures 3** and **4**). As in [22], B-20 Jatropha exhibits high magnitude of velocity for atomization due to viscosity on fuel spray. Hot air presence prior to the fuel injection evaporates the fuel just beyond fixed length (which is called a break-up the length). Engine cylinder spray is around 50–100 atmosphere. At that time, fuel is injected into the chamber. Since the high-

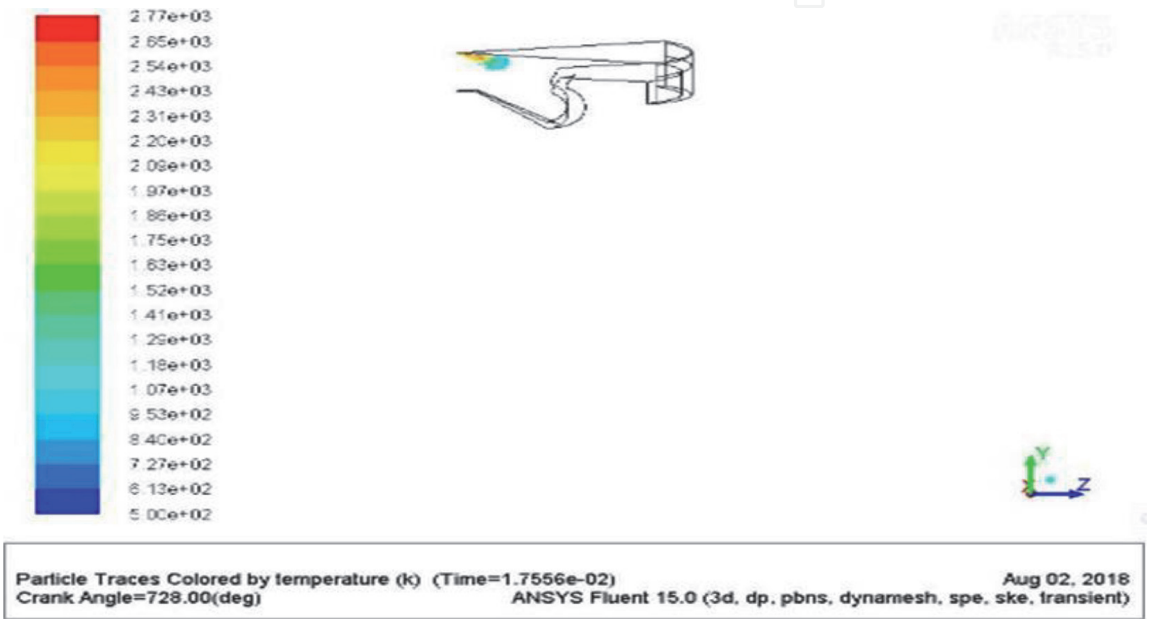


Figure 3.
Visualization of spray at 728° for diesel.

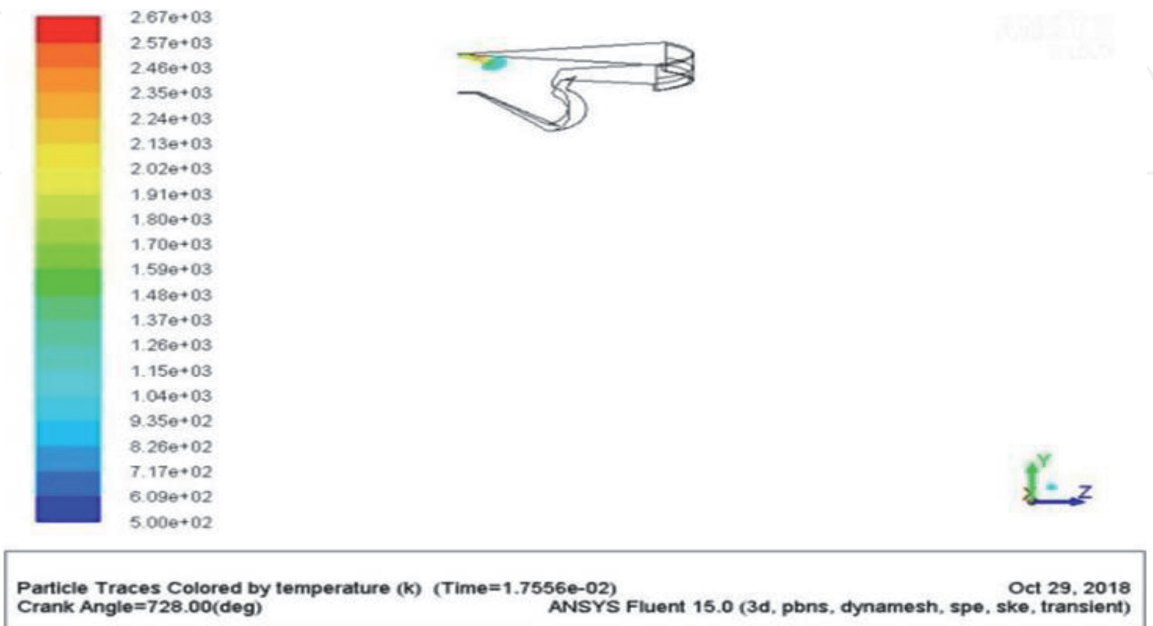


Figure 4.
Visualization of spray at 728° for B-20 Jatropha.



Figure 5.
Velocity contour plot at the time of spray for diesel.



Figure 6.
Velocity contour plot at the time of spray for B-20 Jatropha.

velocity jet has to mix with compressed air in a small interval of time thereby B-20 blend exhibits slightly low velocity magnitude (see **Figures 5 and 6**).

Fuel injection starts at 724°C and ends at 740°C. During fuel injection temperature varies from 500 to 2770°C. But at the end of the compression stroke, diesel temperature varies from 500 to 2360°C, whereas biodiesel temperature varies from 500 to 2180°C. Since B-20 blend is having less heat of vaporization when compared to that of diesel, heat transfer lowers the local air temperature as observed in [23]. Similarly, the magnitude of velocity for B-20 blend is slightly lower than that of diesel (see **Figures 5 and 6**).

Figures 7 and 8 show the variation of temperature after the combustion for diesel and B-20 Jatropha. Temperature varies from 443 to 705°C for the diesel, whereas it varies from 437 to 685°C for biodiesel. Slightly low temperature variation is noticed for the B-20 blend. This could be due to high diffusion burning phase for

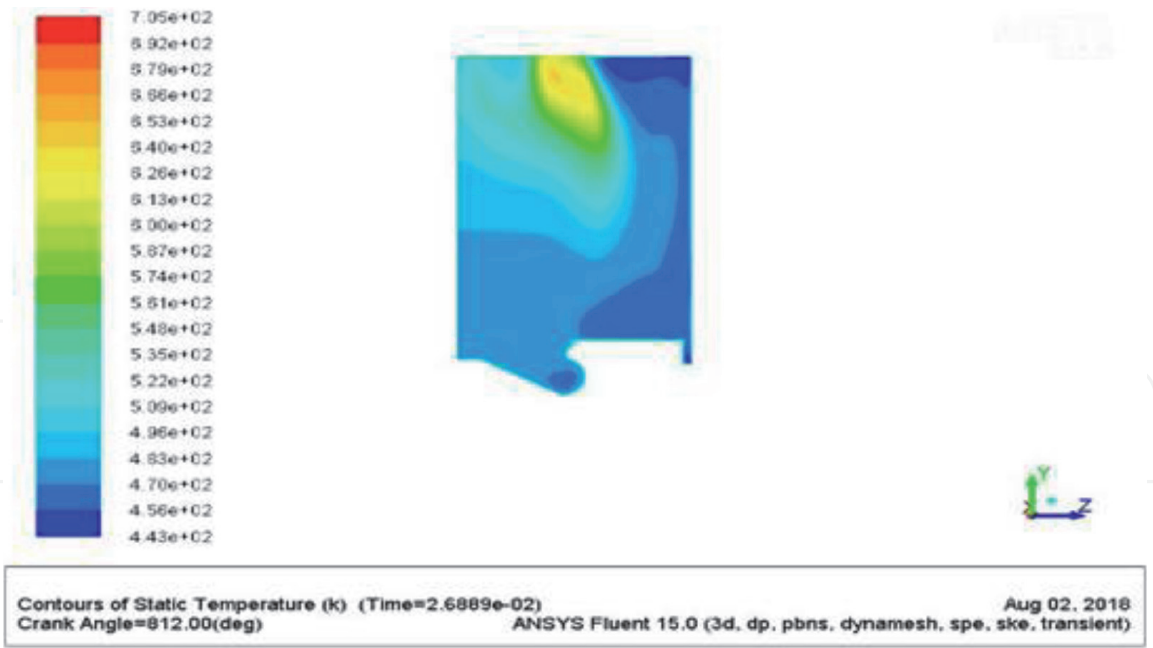


Figure 7.
Temperature distribution after combustion for diesel.

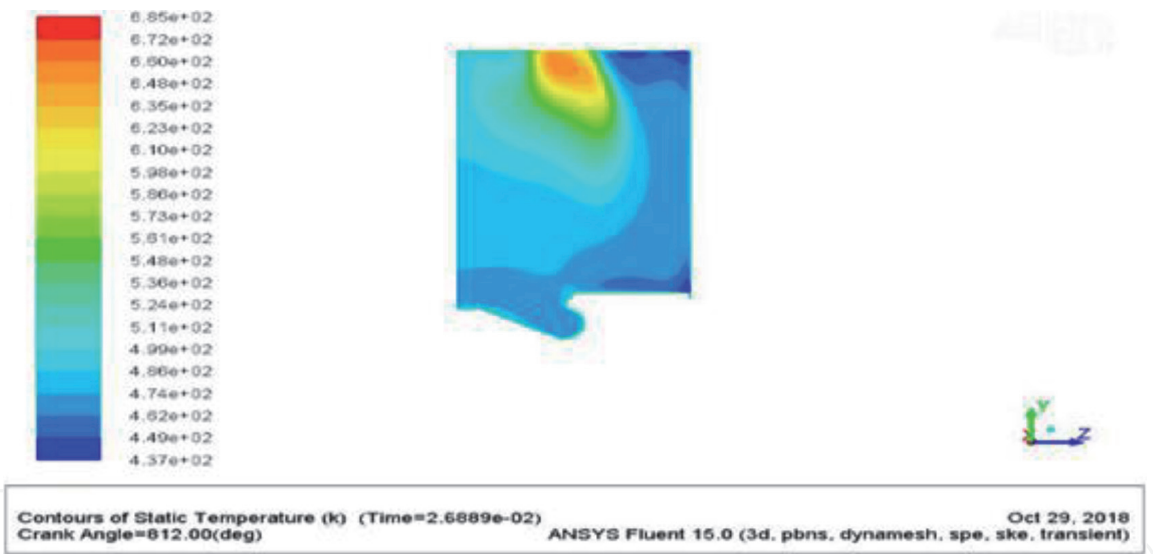


Figure 8.
Temperature distribution after combustion for B-20 Jatropha.

the biodiesel. Due to increase in volatility of the slow-burning biodiesel, burning time is significantly high for B-20 as in [24].

It is noted at the end of the expansion stroke that the velocity magnitude for diesel varies up to 9.34 m/s, whereas in case of B-20 blend, it varies up to 9.4 m/s. Some amount of residual gases present in the engine at the end of expansion stroke.

3. Differential Scanning Calorimetry (DSC) Experiments

DSC experiments are performed under air atmosphere to diesel, Jatropha oil methyl ester (JOME), and its B-20 blend at 10°C/min in Universal TA instruments with alumina pan. Performing experiments on liquid samples is difficult due to evaporation and non-stability of complex during heating. Hermetically sealed pans

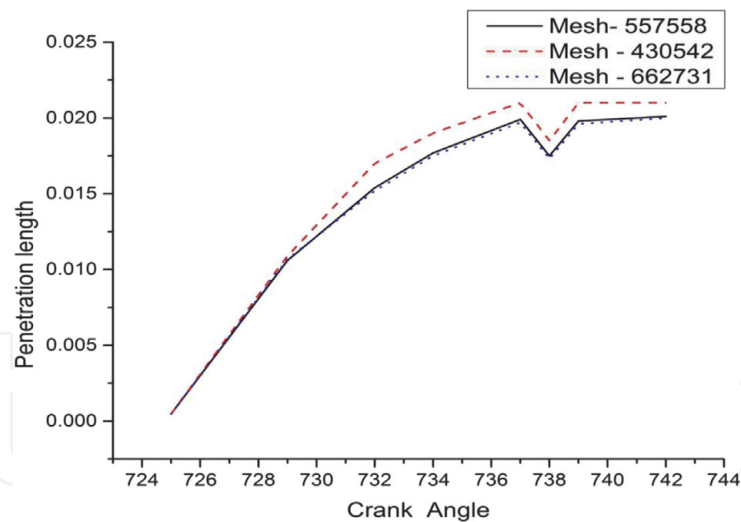


Figure 9.
 Mesh Convergence study.

are used in experiments with universal crammer. Two types of calibration are performed on instrument: (i) Initially with T-Zero (Temperature) calibration; and (ii) Enthalpy calibration. Initially Experiments are performed without the samples to get baseline further with known material (sapphire or Al_2O_3) heat of fusion is calculated by heating up to its melting point. Heat of fusion value is compared with theoretical estimates.

4. Mesh convergence study

Convergence study is made by varying mesh (See **Figure 9**). Computational domain is chosen for three different meshes (430,542, 557,558 and 662,731). Maximum deviation of 9.4% is observed in results by increasing the number of meshes from 430,542 to 557,558. Further increasing to 662,731, maximum deviation of 1.3% is observed. From this study, number of meshes finalized for computation is 557,558.

5. Results and discussion

Deformation on the working fluid increases due to viscous shear stress. Thereby its internal energy increases at the expense of its turbulent kinetic energy. During compression, the airflow is forced into the piston and the swirl rotational velocity increases at the end of the compression stroke. The radius is reduced while the momentum is conserved leading to increase in angular velocity. When the piston moves down, reverse trend happens. The flow slows down due to the friction against the combustion chamber walls [25].

Velocity magnitude in **Figure 10** shows little variation from 570° to 725° and large variation where injection starts at 725° and ends at 748° . Biodiesels show slightly low velocity magnitudes resulting in the time delay. The penetration length in **Figure 11** can be divided into 3 phases as in. [26]. In the initial phase, there is no penetration length (i.e., zero) for the crank angles from 722° to 725° . In the second phase, the penetration length increases rapidly from starting to ending of injection period for the crank angles from 725° to 737° , which indicates more amount of fuel injected inside the engine cylinder. Similar phenomenon is observed for the biodiesel with less penetration length.

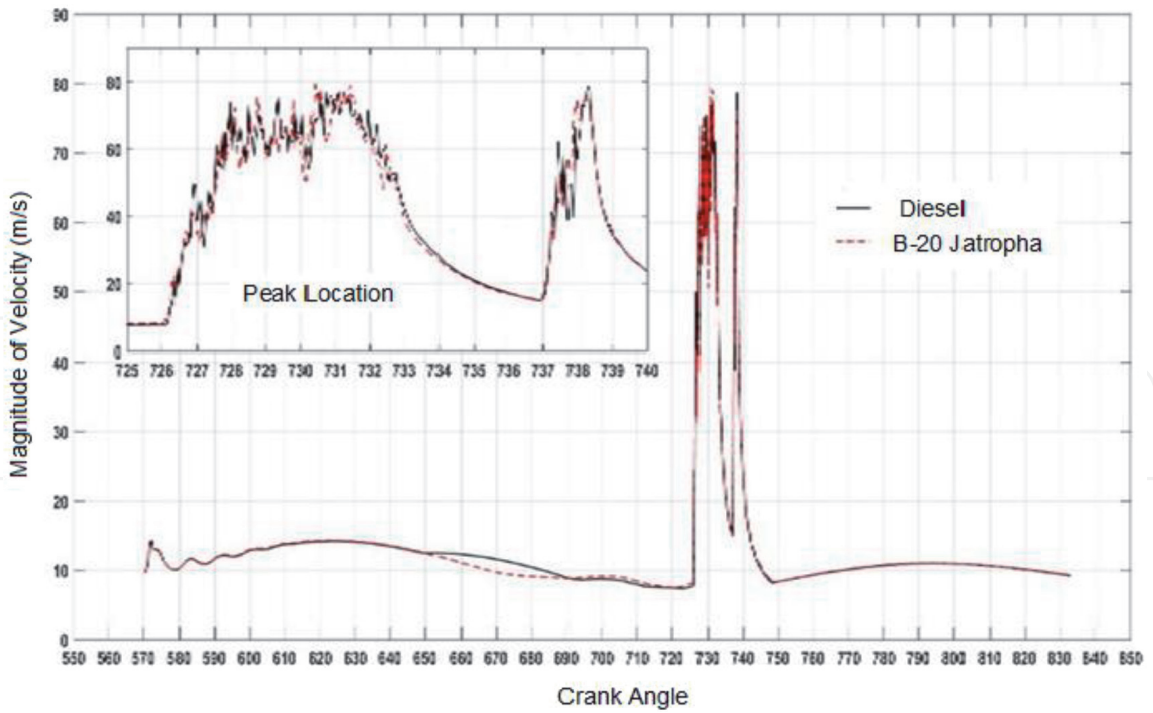


Figure 10.
Magnitude of velocity versus crank angle.

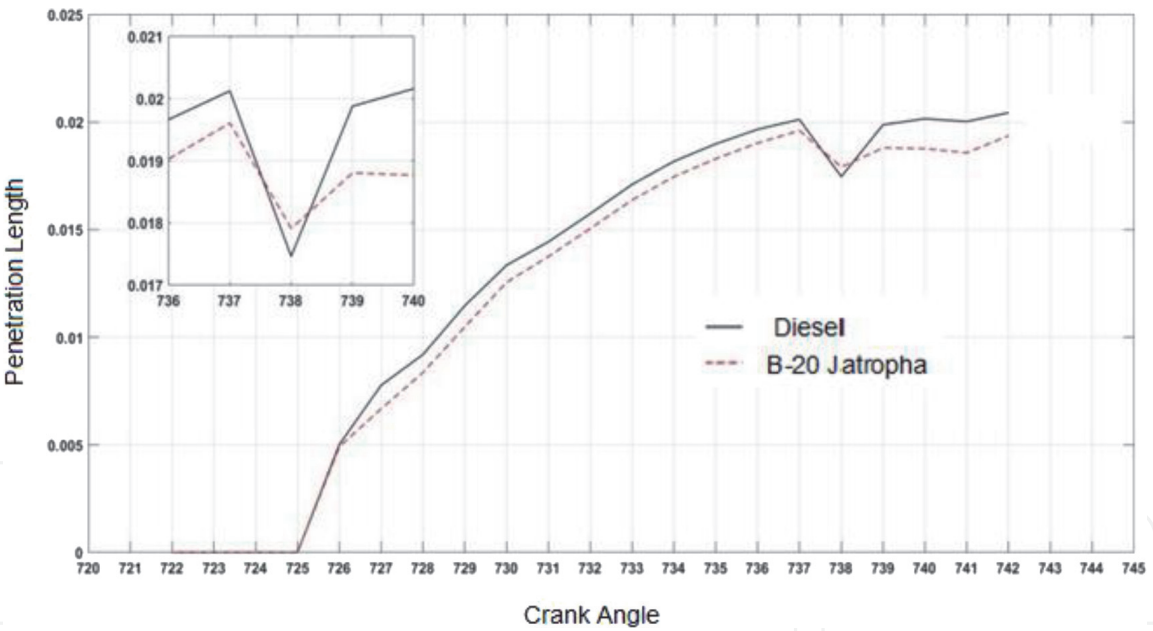


Figure 11.
Penetration length versus Crank angle.

Turbulence is of the major concern in the engine cylinder. The diffusion in the engine cylinder results from the local fluctuations in the flow field. This leads to the enhanced rates of momentum, heat and mass transfer yielding to the satisfactory engine operation. The engine flows involve complicated shear layer combination, boundary layer, and reticulating regions [27]. As the flow is unsteady it exhibits cycle by cycle fluctuations. In diesel engine swirl is used for rapid mixing between the inducted charge and the injected fuel. It is also used for speeding the combustion process. **Figure 12** shows the swirl ratio versus crank angle for diesel and B-20 Jatropa. For diesel and biodiesel compression starts at 570.25 deg. crank angle with a temperature of 404°C and ends at 712° CA with temperature 1008°C, Swirl ratio varies from 1.3 to 0.89 during the CA 570° to 830° for the biodiesel swirl ratio varies

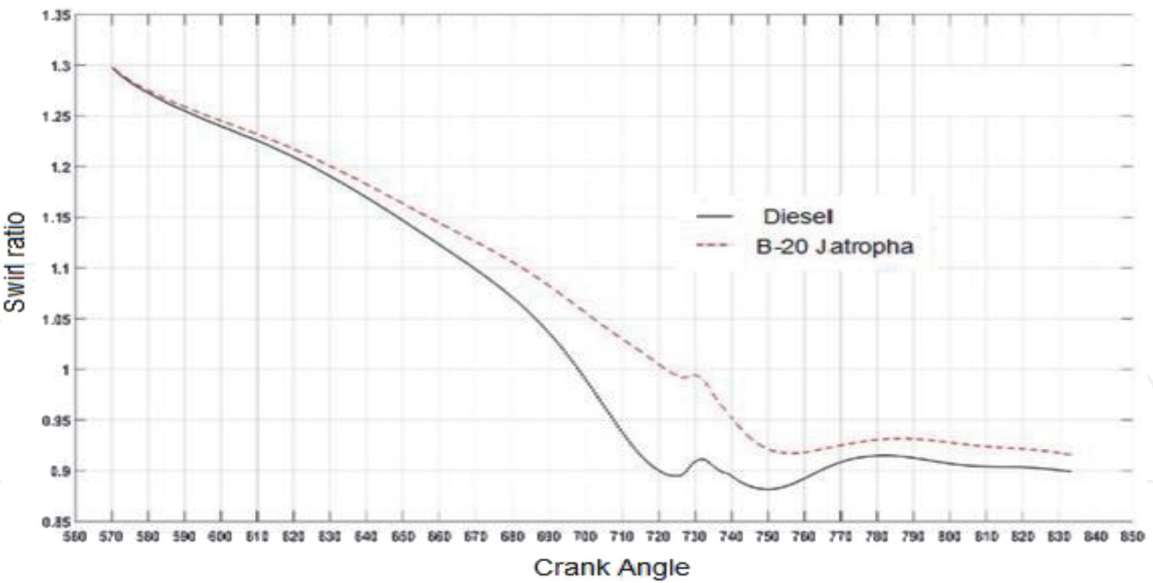


Figure 12.
Swirl ratio versus crank angle.

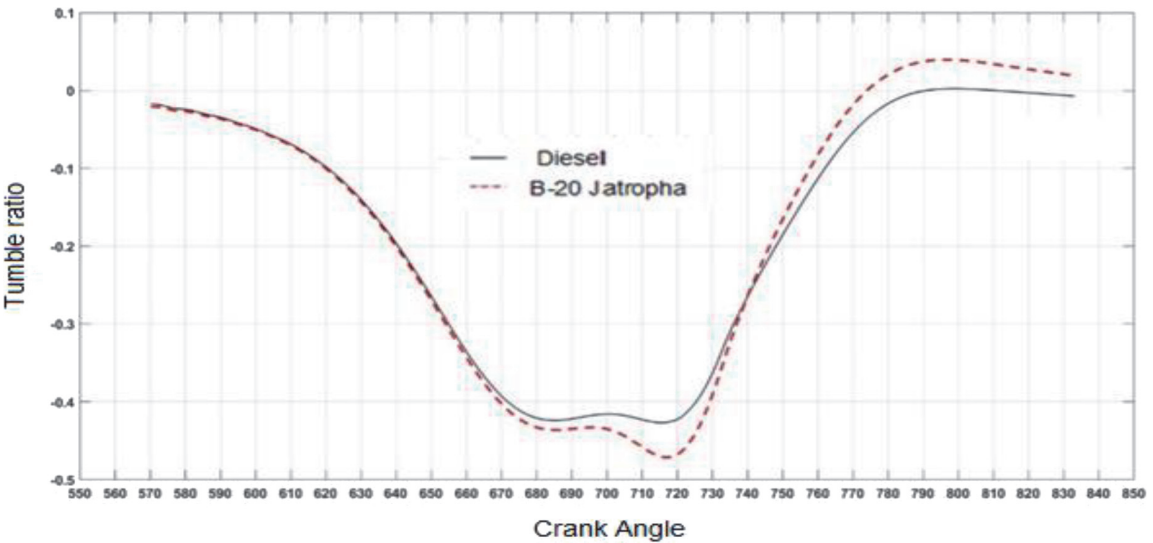


Figure 13.
Tumble ratio versus crank angle.

from 1.3 to 0.92 with same crank angle. B-20 JOME is having high viscosity when compared to that of diesel, which may lead to the complicated shear layer combination thereby increasing the thickness of the boundary layer.

Tumble ratio strongly affects the mixture formation. The high-pressure fuel injection certainly disturbs the bulk motion of the cylinder in the engine. The effect of fuel injection pressure on bulk motion of air is negligible because of symmetrical positioning of the fuel injector holes about the axis of the injector. The tumble ratio in **Figure 13** decreases (from -0.03 to -0.42) initially from 570° to 700° CA and again increases (from -0.42 to 0) during the combustion stroke (i.e., from 720 to 800° CA). In case of B-20 JOME, tumble ratio decreases from -0.03 to 0.44 and increases from 0.44 to 0.03 . For biodiesel tumble ratio, there are some fluctuations from 700° to 720° CA. During that situation, piston is nearer to the TDC and fuel injection happens period. This phenomenon may be due to the presence of oxygen content in biodiesels leading to the oxidation process. This behaviour can be noticed from the temperature contour plot for diesel and biodiesel. Tumble ratio does not vary much till certain crank angle degree and for the reduced volume of high

combustion chamber. Tumble ratio is found to be high at high engine speeds during the fuel injection phase because of high piston velocity helping tumble motion [28]. Peak pressure rise depends on the combustion rate during the initial phase. In turn it depends on the amount of fuel present in the uncontrolled combustion phase. The volatility of the slow-burning biodiesel increases the combustion duration thereby giving the high rate of pressure rise (see **Figure 14**).

Premixed burning phase associated with high heat release rate is significant to the diesel. It gives high thermal efficiency for the diesel. **Figure 15** shows apparent heat release rate (AHRR) versus crank angle. From the heat release rate graph, one can analyse the occurrence of short premixed heat release flame for the esters. Diffusion burning phase under the second peak is high for biodiesel when compared to that of diesel. This may be due to viscosity of biodiesels on fuel spray, reduction of air entrainment and fuel-air mixing rates. Biodiesels possess low latent heat of vaporization. Thereby, heat transfer lowers local air temperature [29]. The heat release rate for the biodiesel is found to be low when compared to that of diesel.

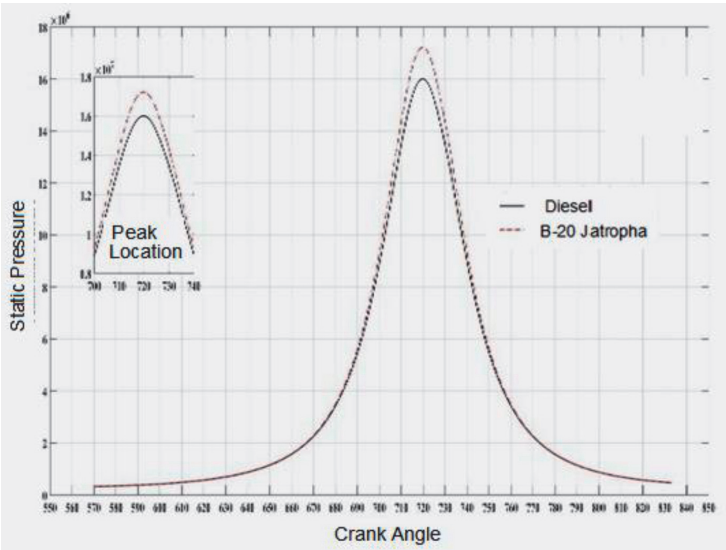


Figure 14.
Static pressure versus crank angle.

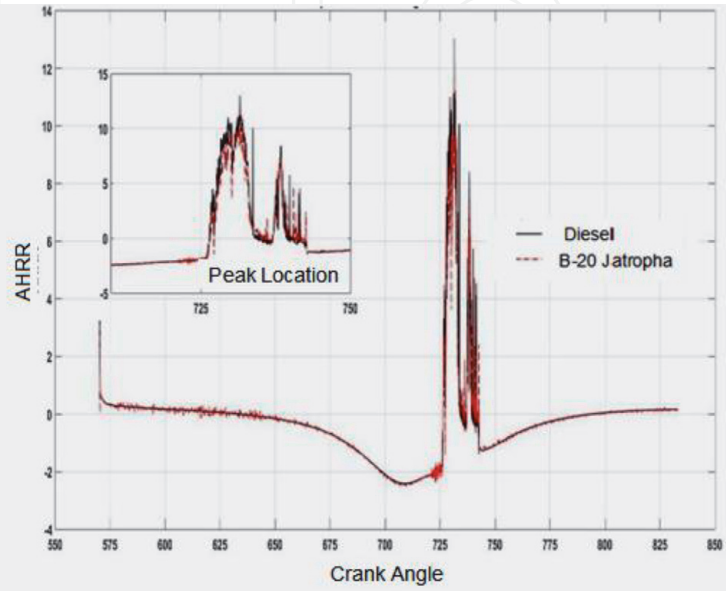


Figure 15.
Apparent heat release rate (AHRR) versus crank angle.

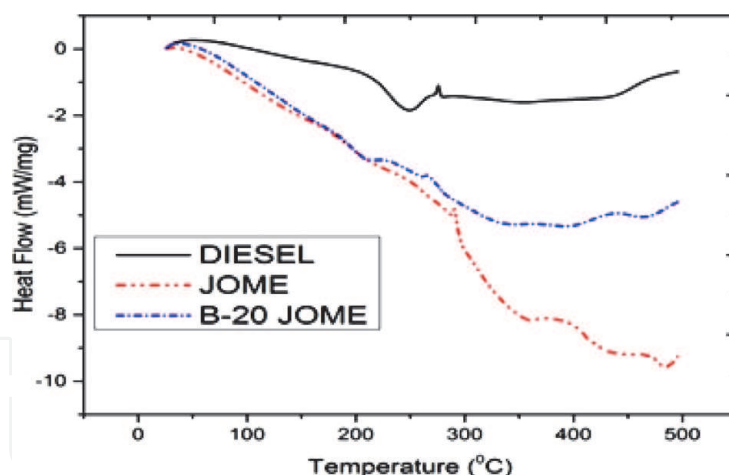


Figure 16.
Comparison of DSC Combustion curves.

Figure 16 shows the comparison of DSC combustion curves. Generally, combustion process of organic fuels exhibit exothermic reaction in air due to double bond presence [30]. JOME consists of the carbon number varying from 14 to 20 (i.e., C_{14} to C_{20}) which decomposes in the range of 30–240°C. JOME exhibits 298°C peak temperature of combustion with 84 J/g enthalpy. Biodiesel in engine results in hard burning with less enthalpy [31, 32]. Combustion curve of B-20 exhibits 268°C peak temperature with 147.5 J/g enthalpy, which is comparable to that of diesel having 138 J/g enthalpy. This indicates that combustion of B-20 JOME is close to that of diesel. Combustion of diesel molecules takes place initially followed by biodiesel [33, 34]. B-20 JOME combustion starts early resulting in better combustion when compared to JOME and diesel with high reaction region. During the initial phase of biodiesel combustion short pre-mixed flame occurs followed by diffusion burning phase requiring blending [34]. B-20 JOME indicates that JOME and diesel molecules mixed perfectly and homogenous mixture occurs at 20%. Therefore, performance of B-20 blend is close to that of diesel.

6. Conclusions

Combustion simulations are performed on the four-stroke single-cylinder direct injection compression ignition engine running at a constant speed of 1500 rpm, injection timing of 25° BTDC with diesel and 20% blend of Jatropha biodiesel. Standard FVM (finite volume method) of CFD (computational fluid dynamics) is considered while simulating the two-phase engine flow. 3-Dimensional N-S (Navier–Stokes) equations are solved with k- ϵ turbulence model.

- Results of combustion simulations are presented for half-cycle by considering the two strokes compression and expansion at zero load condition. *The physiochemical properties of B-20 blend differ significantly with those of diesel. The processes like fuel injection, mixture propagation, and combustion differ significantly. For 570° to 830° CA, swirl ratio varies from 1.3 to 0.89 for diesel, whereas it varies from 1.3 to 0.92 for B-20 JOME. For 720°–800° CA, tumble ratio decreases from –0.03 to –0.42 and increases to zero during the combustion stroke. For B-20 JOME, tumble ratio decreases from –0.03 to –0.44 and increases to –0.03 for the same CA. Some fluctuations are observed in the biodiesel tumble ratio from 700° to 720°CA.*

- Combustion simulations confirm the B-20 blend as an alternative for diesel. DSC profiles of the diesel and B-20 JOME show endothermic peak, which is related to vaporization of methyl esters for B-20 JOME and volatilization of small fraction for the diesel.
- Biodiesel exhibits high enthalpy despite combustion of the engine, and causing serious engine problems. B-20 blend exhibits high enthalpy when compared to that of diesel with reduced peak temperature. Biodiesel exhibits high enthalpy despite of satisfactory performance as a fuel, its high viscosity causing poor fuel atomization. The trend of simulations matches with DSC results.

Acknowledgements

The authors would like to acknowledge the encouragements received from the Visvesvarayya Technological University Belgaum and the Koneru Lakshmaiah Educational Foundation, deemed to be University, Vaddeswaram, India.

Conflict of interest

The authors declare that there is no conflict of interests.

Author details

Vinay Atgur^{1,2}, Gowda Manavendra¹, Gururaj Pandurangarao Desai³ and Boggarapu Nageswara Rao^{2*}


¹ Department of Mechanical Engineering, Bapuji Institute of Engineering and Technology (BIET), Davangere, Karnataka, India

² Department of Mechanical Engineering, Koneru Lakshmaiah Education Foundation (KLEF), Deemed to be University, Guntur, Andhra Pradesh, India

³ Department of Chemical Engineering, Bapuji Institute of Engineering and Technology (BIET), Davangere, Karnataka, India

*Address all correspondence to: bnrao52@rediffmail.com

IntechOpen

© 2022 The Author(s). Licensee IntechOpen. This chapter is distributed under the terms of the Creative Commons Attribution License (<http://creativecommons.org/licenses/by/3.0>), which permits unrestricted use, distribution, and reproduction in any medium, provided the original work is properly cited. 

References

- [1] Kumar N, Ram S. Performance and emission characteristics of biodiesel from different origins: A review. *Renewable and Sustainable Energy Reviews*. 2013;**21**:633-658. DOI: 10.1016/j.rser.2013.01.006
- [2] Rajasekar E, Selvi S. Review of combustion characteristics of CI engines fueled with biodiesel. *Renewable and Sustainable Energy Reviews*. 2014;**35**: 390-399. DOI: 10.1016/j.rser.2014.04.006
- [3] Manaf ISA, Embong NH, Khazaai SNM, Rahim MHA, Yusoff MM, Lee KT, et al. A review for key challenges of the development of biodiesel industry. *Energy Conversion and Management*. 2019;**185**:508-517
- [4] Jafarmadar S, Zehni A. Combustion modeling for modern direct injection diesel engines. *Iranian journal of chemistry and chemical engineering*. 2012;**31**(3):111-114
- [5] Griend LV, Feldman ME, Peterson CL. Modeling combustion of alternative fuels in a DI diesel engine using KIVA. *Transactions of the ASABE*. 1988;**33**(2):342-350. DOI: 10.13031/2013.31336
- [6] Cantrell BA, Reitz RD, Rutland CJ, Imamore Y. Strategies for reducing the computational time of diesel engine CFD simulations. In: *International Multidimensional Engine Modeling User's Group Meeting*. (SAE Congress, 23 April 2012), Warrendale, PA, USA: SAE International; 2012
- [7] Fukuda K, Ghasemi A, Barron R, Balachandar R. An Open Cycle Simulation of DI Diesel Engine Flow Field Effect on Spray Processes. Warrendale, PA, USA: SAE International. SAE Technical Paper 2012-01-06962012. DOI: 10.4271/2012-01-0696
- [8] Dimitriou P, Tsujimura T, Kojima H, Aoyagi K, Kurimoto N. Experimental and simulation analysis of natural gas-diesel combustion in dual-fuel engines. *Frontiers in Mechanical Engineering*. 2020;**6**:1-14. DOI: 10.3389/fmech.2020.543808
- [9] Baratta M, Chiriches S, Goel P, Misul D. CFD modelling of natural gas combustion in IC engines under different EGR dilution and H₂-doping conditions. *Transportation Engineering*. 2020;**2**:1-12. DOI: 10.1016/j.treng.2020.100018
- [10] Costa M, Piazzullo D. Biofuel powering of internal combustion engines: Production routes, effect on performance and CFD modeling of combustion. *Frontiers of Mechanical Engineering*. 2018;**4**:9. DOI: 10.3389/fmech.2018.00009
- [11] Maghbouli A, Khoshbakhti R, Shafee S, Ghafouri J. Numerical study of combustion and emission characteristics of dual-fuel engines using 3D-CFD models coupled with chemical kinetics. *Fuel*. 2013;**106**:98-105. DOI: 10.1016/j.fuel.2012.10.055
- [12] Vijayashree GV. Application of CFD for analysis and design of IC engines. In: *Srivastava D, Agarwal A, Datta A, Maurya R, editors. Advances in Internal Combustion Engine Research*. Energy, Environment, and Sustainability. Singapore: Springer; 2018. DOI: 10.1007/978-981-10-7575-9_13
- [13] Salam S, Choudhary T, Pugazhendhi A, Verma TN, Sharma A. A review on recent progress in computational and empirical studies of compression ignition internal combustion engine. *Fuel*. 2020;**279**: 118469. DOI: 10.1016/j.fuel.2020.118469

- [14] Kerstein AR. Turbulence in combustion processes: Modeling challenges. Proceedings of the Combustion Institute. 2002;**29**(2): 1763-1773. DOI: 10.1016/s1540-7489(02)80214-0
- [15] Zhou LX. Advances in studies on two-phase turbulence in dispersed multiphase flows. International Journal of Multiphase Flow. 2010;**36**(2): 100-108. DOI: 10.1016/j.ijmultiphaseflow.2009.02.011
- [16] Azad AK, Rasul MG, Khan MMK, Sharma SC, Bhuiya MMK. Recent development of biodiesel combustion strategies and modelling for compression ignition engines. Renewable and Sustainable Energy Reviews. 2016;**56**:1068-1086. DOI: 10.1016/j.rser.2015.12.024
- [17] Sasidhar Saketh AVS, Raja M, Nageswara RB. Selection of a suitable turbulent model in CFD codes to perform simulations for a circular microchannel heat exchanger. International Journal of Mechanical and Production Engineering Research and Development (IJMPERD), Special Issue. Aug 2018:608-623
- [18] Basha SA, Gopal KR. In-cylinder fluid flow turbulence and spray models. Renewable and Sustainable Energy Reviews. 2008;**13**(6-7):1620-1627
- [19] Sharma CS, Anand TNC, Ravikrishna RV. A methodology for analysis of diesel engine in-cylinder flow and combustion. Progress in Computational Fluid Dynamics. 2010; **10**(3):157-167. DOI: 10.1504/PCFD.2010.033327
- [20] Gugulothu SK, Reddy KHC. CFD simulation of in-cylinder flow on different piston bowl geometries in a DI diesel engine. Journal of Applied Fluid Mechanics. 2016;**9**(3):1147-1155. DOI: 10.18869/acadpub.jafm.68.228.24397
- [21] Zellat M., Abouri D. and Conte T. (2014). Advanced Modeling of DI Diesel Engines Investigations on Combustion, High EGR Level and Multiple- Injection Application to DI Diesel Combustion Optimization. https://www.energy.gov/sites/prod/files/2014/03/f9/2005_deer_zellat.pdf
- [22] Posom J, Sirisomboon P. Evaluation of the thermal properties of *Jatropha curcas* L. kernels using near-infrared spectroscopy. Biosystems Engineering. 2014;**125**:45-53. DOI: 10.1016/j.biosystemseng.2014.06.011
- [23] Kongre UV, Sunnapwar VK. CFD modeling and experimental validation of combustion in direct ignition engine fueled with diesel. International Journal of Applied Engineering Research. 2010; **1**(3):508-517
- [24] Imamore Y, Hiraoka K. Combustion simulations contributing to the development of reliable low-emission diesel engines. Mitsubishi Heavy. 2011; **48**(1):65-69 <http://www.mhnglobal.com/company/technology/review/pdf/e481/e481065.pdf>
- [25] Paul G, Datta A, Mandal BK. An experimental and numerical investigation of the performance, combustion and emission characteristics of a diesel engine fueled with *jatropha* biodiesel. Energy Procedia. 2014;**54**: 455-467. DOI: 10.1016/j.egypro.2014.07.288
- [26] Dembinski HWR. In-cylinder Flow Characterisation of Heavy Duty Diesel Engines Using Combustion Image Velocimetry. Mumbai, India: Integrated Publishing Association. 2013. DOI: 10.1016/j.radonc.2014.09.010
- [27] Mirmohammadi A, Ommi F. Internal combustion engines in-cylinder flow simulation improvement using nonlinear k- ϵ turbulence models. Journal of Computational and Applied

Research in Mechanical Engineering.
2015;**5**(1):61-69

[28] Raj RTK, Manimaran R. Effect of swirl in a constant speed DI diesel. *CFD Letters*. 2012;**4**:214-224

[29] Banapurmath NR, Tewari PG. Performance, combustion, and emissions characteristics of a single-cylinder compression ignition engine operated on ethanol-biodiesel blended fuels. *Proceedings of the Institution of Mechanical Engineers, Part A: Journal of Power and Energy*. 2010;**224**(4): 533-543. DOI: 10.1243/09576509JPE850

[30] Mohammed MN, Atabani AE, Uguz G, Lay CH, Kumar G, Al-Samarae RR. Characterization of Hemp (*Cannabis sativa* L.) biodiesel blends with Euro diesel, butanol and diethyl ether using FT-IR, UV-Vis, TGA and DSC techniques. *Waste and Biomass Valorization*. 2020;**11**(3):1097-1113. DOI: 10.1007/s12649-018-0340-8

[31] Dinkov R, Hristov G, Stratiev D, Boynova AV. Effect of commercially available antioxidants over biodiesel/diesel blends stability. *Fuel*. 2009;**88**(4): 732-737. DOI: 10.1016/j.fuel.2008.09.017

[32] Vossoughi S, El-Shoubary YM. Kinetics of liquid hydrocarbon combustion using the DSC technique. *Thermochimica Acta*. 1990;**157**(1): 37-44. DOI: 10.1016/0040-6031(90)80004-I

[33] Vinay Atgur G, Manavendra GPD, Nageswara Rao B. Thermal characterization of dairy washed scum methyl ester and its b-20 blend for combustion applications. *International Journal of Ambient Energy*. 2021 (in Press). DOI: 10.1080/01430750.2021.1909651

[34] Almazrouei M, Janajreh I. Thermogravimetric study of the combustion characteristics of biodiesel

and petroleum diesel. *Journal of Thermal Analysis and Calorimetry*. 2019;**136**(2):925-935. DOI: 10.1007/s10973-018-7717-6